energies

MDPI

Article

A Study of the Energy Exchange within a Hybrid Energy Storage System and a Comparison of the Capacities, Lifetimes, and Costs of Different Systems

Yang Jiao * and Daniel Månsson

Division of Electromagnetic Engineering, KTH Royal Institute of Technology, SE-100 44 Stockholm, Sweden; manssond@kth.se

* Correspondence: yjiao@kth.se

Abstract: By combining the advantages of different energy storage technologies, the hybrid energy storage system (HESS) can satisfy the multiple requirements of prosumer systems. However, the required capacity of the HESS is larger than that of the single-battery energy storage system (ESS). This paper investigates the energy exchange within the HESS caused by the phase shift of the low-pass filter controller and its relevant impact on the HESS. The results show that unnecessary energy exchange results in an oversized capacity and increased energy loss. In addition, the increase in the time constant of the low-pass filter controller leads to a larger phase shift, further contributing to the increases in the total capacity and energy loss. Furthermore, this paper compares the single-battery ESS, the battery-supercapacitor HESS, and the battery-flywheel HESS implemented in a household-prosumer system along with a renewable energy source (RES). The comparison of the ESS combinations demonstrates the differences between their power flows, the required capacities of their individual energy storage devices (ESDs), their energy losses, their battery lifetimes, and their project costs. The results indicate that techno-economic analysis should be performed carefully to select the appropriate ESS solution for specific household-prosumer systems.

Keywords: battery; energy exchange; household-prosumer system; hybrid energy storage system (HESS); oversized capacity; phase shift; supercapacitor (SC)

check for updates

Citation: Jiao, Y.; Månsson, D. A Study of the Energy Exchange within a Hybrid Energy Storage System and a Comparison of the Capacities, Lifetimes, and Costs of Different Systems. *Energies* **2021**, *14*, 7045. https://doi.org/10.3390/en14217045

Academic Editor: Adalgisa Sinicropi

Received: 28 September 2021
Accepted: 22 October 2021
Published: 28 October 2021

Publisher's Note: MDPI stays neutral with regard to jurisdictional claims in published maps and institutional affiliations.

Copyright: © 2021 by the authors. Licensee MDPI, Basel, Switzerland. This article is an open access article distributed under the terms and conditions of the Creative Commons Attribution (CC BY) license (https://creativecommons.org/licenses/by/4.0/).

1. Introduction

Distributed renewable energy sources (RESs), represented by photovoltaic (PV) and wind power generation, have developed rapidly in recent decades. Prosumer systems can utilize RESs generation locally (i.e., self-production and self-consumption), which increases renewable energy penetration. However, the output power of RESs is easily affected by the environment and features relatively poor stability, weak continuity, and low reliability. In addition, there are spatial and temporal gaps between intermittent energy and its consumption, which causes an imbalance between the available RESs and their end users [1,2]. These problems challenge the stability and power quality of prosumer systems. To overcome the intermittent aspect of RESs, introducing an energy storage system (ESS) is an effective approach for suppressing power fluctuations, achieving load shifting, and improving stability and reliability [3].

Currently, there is no single energy storage technology that fully satisfies the multiple requirements of prosumer systems, such as high energy and high power density, short response time, long lifetime, and low cost. Energy storage devices (ESDs) with a high energy density usually have a relatively larger storage capacity but a slower response time and a lower lifecycle [4]. For example, the capacity of Li-ion batteries fades when the charging/discharging operation employs high frequencies [5]. In addition, redox flow batteries are usually cost-effective, but they require long-term usage and large-scale applications [6,7]. By contrast, supercapacitors (SCs) and flywheels can quickly respond

to high power demands and feature long lifetimes, which are suitable for small-scale applications with rapid charge and discharge requirements. Thus, the concept of hybrid energy storage systems (HESSs), which combine the advantages of different energy storage technologies, is a promising solution for research and applications. A HESS usually consists of two individual ESDs: one ESD features high energy density for primary storage, e.g., fuel cells or batteries, and the other ESD features a high power density for secondary storage, e.g., SCs or flywheels. Synergies are achieved by combining the different advantages of the two ESDs, i.e., by providing both high power and high energy density [4,8].

Due to the various frequency and amplitude fluctuations of the power demands in RES prosumer applications, a control strategy of a HESS that adequately handles both low- and high-frequency power responses is preferable. Consequently, the filtration-based controller is one of the most widely used control strategies for distributing the power demand of HESSs, since it is simple and easy to utilize and tune [9]. However, its disadvantage is the unavoidable phase shift from its linear filter controllers [10]. As a result, the total required capacity of the HESS is larger than that of the single-battery ESS [11,12]. Most previous studies have emphasized the benefits of HESSs and the extension of the battery lifetime [13–15]. However, the required capacity of a HESS, particularly due to its oversized capacity and its relevant impact, has not been thoroughly investigated to date. Furthermore, several published studies have developed and introduced different HESSs into prosumer systems [16,17], among which battery-SC HESSs and battery-flywheel HESSs are often utilized to achieve load shifting and energy management [15–17]. Nevertheless, SCs and flywheels feature different working principles and charge/discharge characteristics. Recent attempts to understand HESSs do not fully address these nuances. Specific analyses and comparative studies of battery-SC HESSs and battery-flywheel HESSs are needed.

Although different HESSs have been researched, most studies are restricted to the adjustment of the SOC and dynamic response performance. However, previous studies ignore the oversized capacity problem that stems from the primary filter circuit. No systematic analysis of the association between the required capacity of HESSs and the time constant of the low-pass filter controller has been performed. Clearly, further work is needed to address the oversized capacity problem and to indicate an appropriate approach to the optimization of smart control strategies. Therefore, this paper aims to investigate the energy exchange caused by the phase shift and the relevant impact on the required capacity and energy loss of a HESS. This study will help to address the aforementioned gaps in previous research and provide a reference for selecting the appropriate ESS combinations in RES household-prosumer systems.

In this study, the analysis of the power flows in a HESS explores the time delay that stems from the phase shift of the low-pass filter. The time delay causes an unnecessary energy exchange between the primary ESD and the secondary ESD within the HESS. It leads to increases in the required capacity and energy losses. A scaled-down experimental setup was built to validate the simulation results. In addition, this paper compares the single-battery ESS, the battery-SC HESS, and the battery-flywheel HESS. The comparison discusses these ESS combinations in a stand-alone prosumer application that contains a RES (wind-powered or PV-powered) and a residential load. The lifetimes of the batteries and the project costs for the HESSs are evaluated. The lifetimes of the batteries in the ESS combinations are compared using nickel manganese cobalt oxide (NMC) batteries and lithium iron phosphate (LFP) batteries. The total costs of the ESS combinations that consist of NMC/LFP batteries and SCs/flywheels with a 30 year project lifetime are compared.

This paper is organized as follows. After the introduction in Section 1, Section 2 describes the HESS topology and the control strategy. Section 3 analyses the energy exchange in a simulated HESS, which results in the oversized capacity and increased energy loss of the HESS. In addition, an experimental setup was built to validate the simulations. Section 4 compares the single-battery ESS with the battery-SC HESS and the battery-flywheel HESS in the RES household-prosumer system. Furthermore, the

lifetimes of the batteries and the project costs of the ESS combinations are estimated. Finally, Section 5 provides the conclusions of the study.

2. HESS Topology and Control Strategy

This section presents the details of the HESS topology and the applied controller. A parallel active topology was used. In addition, as the main objective is to investigate the energy exchange between the individual ESDs, a filtration-based controller was applied to control the HESS.

2.1. HESS Topology

HESS topologies can be classified into passive, semi-active, and active topologies [18]. Passive topologies are simple, low-cost, and highly efficient, but cannot be controlled. Semi-active topologies feature a converter at the terminals of one ESD, whereas the other ESD is directly connected to the DC bus. This allows some degree of controllability with a low cost, but cannot utilize all of the capacities of both the ESDs. However, active topologies are capable of flexibly and independently controlling the power flows of both the ESDs. In this study, as shown in Figure 1, a parallel active HESS topology was applied. The primary ESD and the secondary ESD were connected to the DC bus in parallel by the bi-directional DC/DC converters.

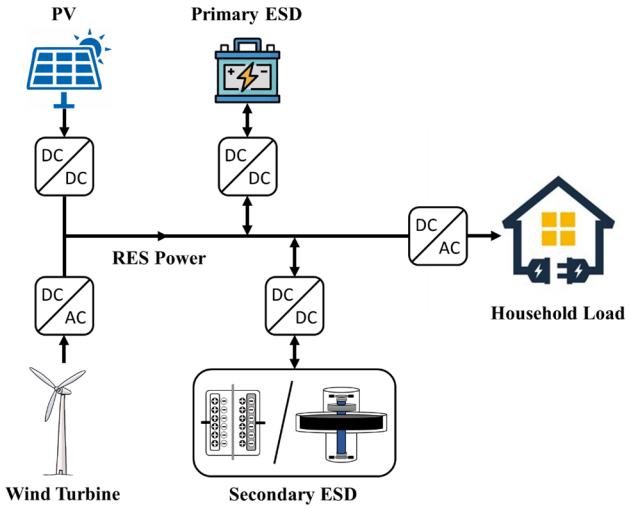


Figure 1. Parallel active HESS configuration in a RES household-prosumer system.

2.2. HESS Control Strategy

Control strategies of HESSs play a vital role in system power balance and voltage regulation. The low-pass filter is the core component in many controllers because it splits the power demand into low- and high-frequency parts [19]. However, linear filtering controllers are often incapable of achieving an optimal power distribution. This can be improved by adding more intelligent control strategies so that the parameter values of the controller can be adjusted. In addition, intelligent algorithms that are even more complex can be implemented to realize multi-parameter and multi-objective optimization, such as neural networks, fuzzy logic controllers, and evolutionary algorithms [20]. Therefore, a conventional low-pass filter controller was used in this study to explore the impact of the energy exchange in the HESSs.

Figure 2 presents the block diagram of the low-pass filter controller. The primary ESD (battery) releases and absorbs the low-frequency power flow, whereas the secondary ESD (SC or flywheel) responds to high-frequency power fluctuations.

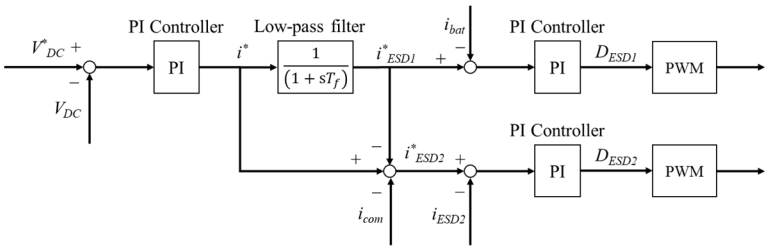


Figure 2. Block diagram of the low-pass filter controller.

The power flows of the two ESDs are given by:

$$\begin{cases} P_{ESD1} = P_{HESS}\frac{1}{1+sT_f} \\ P_{ESD2} = P_{HESS} - P_{ESD1} \end{cases} \quad (1)$$

This power distribution reduces the stress on the primary ESD and thus extends its lifetime. However, the energy stored in the secondary ESD decays with time due to the high self-discharge rate of the SC/flywheel and needs to be compensated. The self-discharge loss of the primary ESD is ignored here due to the relatively low self-discharge rate of the battery.

3. Analysis of Oversized Capacity of HESS

This section discusses and analyzes an example to explore the energy exchange between the individual ESDs and the relevant impact on the required capacity and the energy loss of the HESS.

3.1. Analysis Based on a Simulated Model

A simulated example is presented and analyzed to illustrate the cause of the oversized HESS capacity. The simulation was built in the SimPowerSystem toolbox on the MATLAB-Simulink platform [21]. Figure 3 shows the simulation of the battery-SC HESS in a wind-powered household-prosumer system.

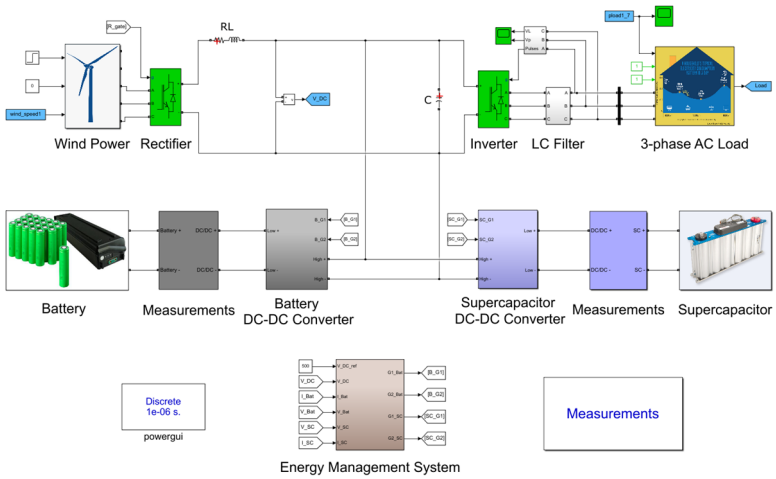


Figure 3. Simulation of the HESS in a household-prosumer system (battery-SC HESS with wind power).

When the output power generated by the RES surpasses the load power, the HESS absorbs the excess power. By contrast, the HESS discharges when the RES output power fails to meet the power demand. The wind speed data used in the simulation were obtained from the Sotavento wind farm [22] in Spain. A 600 W wind turbine was built in the simulation. The PV-powered generation data were obtained from a 2.4 kW PV array

located in southern Sweden [23]. The residential load data profiles were obtained from the Reference Energy Disaggregation Data Set (REDD) [24]. The HESS consists of a 7.2 kWh battery bank and a 1.8 kWh secondary ESD pack (SC or flywheel). The low-pass filter controller introduced in Section 2.2 is used to build the energy management strategy in the simulation.

Figure 4 shows the wind output power, the consumed load power, and the power handled by the HESS.

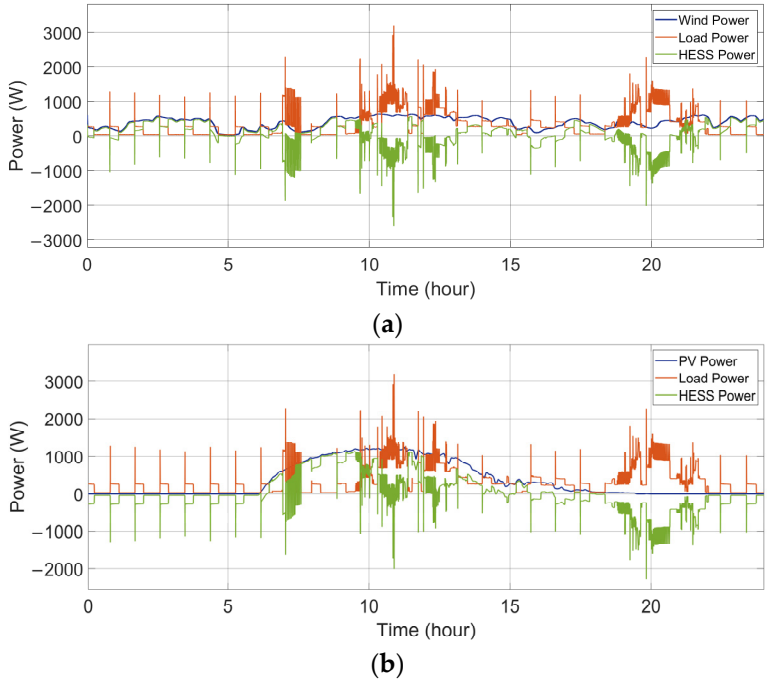


Figure 4. Power flows between the RES, the load, and the HESS. (**a**) Wind-powered household-prosumer system. (**b**) PV-powered household-prosumer system.

The total power flow that needs to be handled by the HESS, ΔP, can be written as:

$$\Delta P = P_{RES} - P_{load} - P_{loss} \tag{2}$$

In the system, the power losses originate from the converters and the ESDs:

$$P_{losses} = (1 - \eta_1)P_{RES} + \left(\frac{1 - \eta_2}{\eta_2}\right)P_{load} + P_{DC/DC_loss} + P_{ESD_loss} \tag{3}$$

To calculate the losses from the converters, the efficiency parameters η_1, η_2, and η_3 are assumed as fixed values. Both the converter efficiencies η_1 and η_2 are set to 97% [25] and the bi-directional DC/DC converter efficiency η_3 is set to 95% [26].

In addition, the losses of the bi-directional DC/DC converters are calculated as:

$$P_{DC/DC_loss} = \begin{cases} (1 - \eta_3) \cdot |P_{ESD}|, \ for \ P_{ESD} < 0 \\ \left(\frac{1-\eta_3}{\eta_3}\right) \cdot |P_{ESD}|, \ for \ P_{ESD} \geq 0 \end{cases} \tag{4}$$

where P_{ESD} represents the power flows of the ESD. The ESD releases power into the system when $P_{ESD} < 0$ and is charged when $P_{ESD} \geq 0$.

In HESSs, the losses of the ESDs mainly stem from cycle losses and self-discharge losses. The series internal resistance causes the cycle losses of the ESDs during charging and discharging. In addition, the equivalent parallel resistance represents self-discharge losses and affects the long-term performance of the ESDs. Most ESDs with high power

density, such as SCs and flywheels, suffer from high leakage rates, which produce a high self-discharge rate.

$$P_{ESD_loss} = P_{cycle_loss} + P_{self\text{-}dis_loss} \quad (5)$$

A comparison of the single-battery ESS and the HESS is presented to illustrate the HESS's behavior. As shown in Figures 5a and 6a, in both the wind-powered and PV-powered household-prosumer systems, when T_f of the low-pass filter is 0 s (single-battery ESS), there is only the battery to handle the entire power demand and the high power peaks. These power peaks correspond to large discharge current rates, which reduce the battery's lifespan. When the time constant T_f is 1800 s, the power flow of the battery in the HESS is smooth. The battery handles fewer power peaks and experiences fewer current polarity reversals. Meanwhile, the SC (or the flywheel) responds to high-frequency power fluctuations, as shown in Figures 5b and 6b. In addition, due to the different power losses in the HESSs, there are slight differences between the power flows in the battery-SC HESS and the battery-flywheel HESS, even though their T_f are the same.

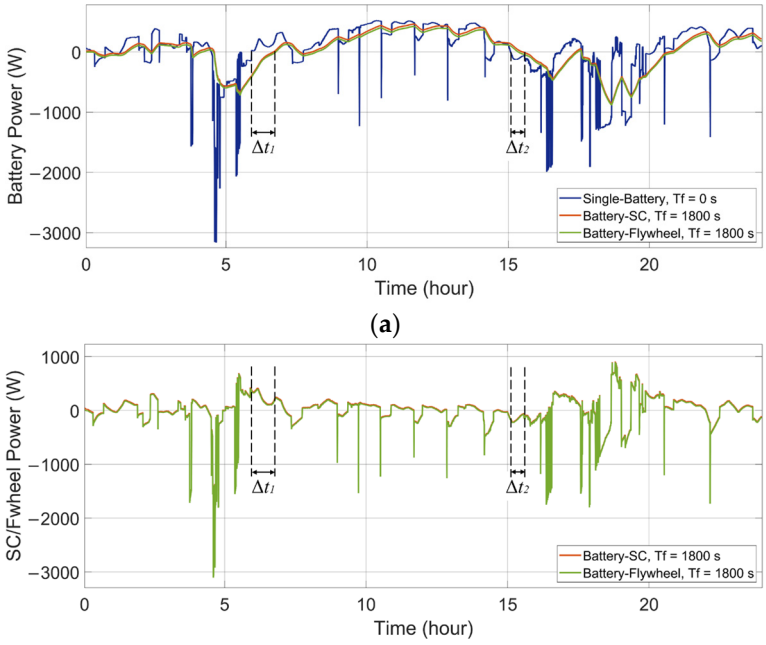


Figure 5. Power flows of the ESDs in the single-battery ESS and the HESSs applied to a wind-powered household-prosumer system. (**a**) Battery power. (**b**) SC/flywheel power.

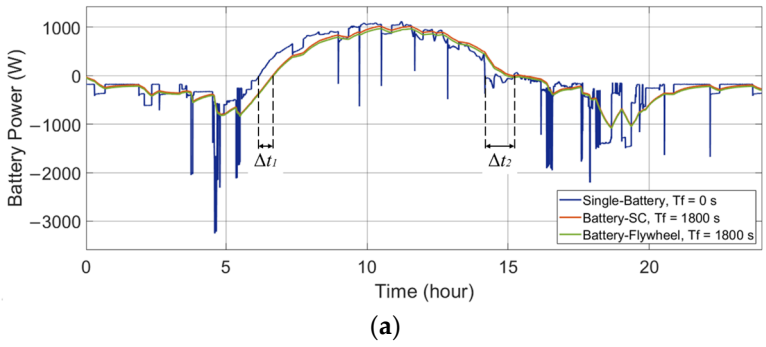
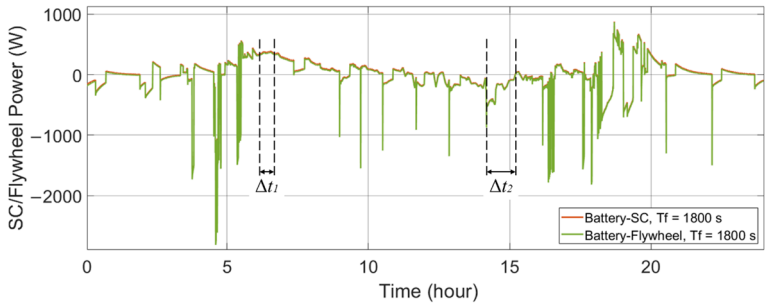


Figure 6. *Cont.*



(**b**)

Figure 6. Power flows of the ESDs in the single-battery ESS and the HESSs applied to a PV-powered household-prosumer system. (**a**) Battery power. (**b**) SC/flywheel power.

In addition, the phase shift of the low-pass filter leads to a time delay in the battery power compared with the original power demand (since the primary ESD is set to respond slowly to the power demand). For example, the time delay, Δt_1 and Δt_2, can be observed at the zero crossing points of the battery power. One ESD charges while the other ESD discharges during these time intervals:

$$\begin{array}{l} P_{bat} > 0,\ P_{SC/flywheel} < 0, \text{ or } P_{bat} < 0,\ P_{SC/flywheel} > 0, \\ \begin{cases} P_{bat} + P_{SC/flywheel} = \Delta P \\ |P_{bat}| + \left|P_{SC/flywheel}\right| > |\Delta P| \end{cases} \end{array} \quad (6)$$

The sum of the absolute values of the ESDs is larger than the absolute value of the original power demand ΔP. It is concluded that there is an energy exchange between the two ESDs. Instead of serving the DC bus, the ESDs deliver energy to each other. Thus, it is unnecessary and not beneficial to the HESS.

The energy states of the individual ESDs in the HESS are plotted in Figures 7 and 8. The deviation between the maximum point and the minimum point of the curve is:

$$\Delta E = E_{\max} - E_{\min} \quad (7)$$

where ΔE is thus the maximum deviation of the energy states over the testing interval, i.e., the available capacity of the ESD to meet the power demand. The ΔE of the ESD determines the required installed capacity and thus the cost of the HESS, which are discussed in Section 4. In addition, it should be noted that, due to the comparison between various energy storage technologies, the unit representing the capacities of the different ESDs is uniformly converted to represent energy (Wh).

Figures 7a and 8a present the battery energy states for the batteries in the ESS combinations in the wind-powered and PV-powered household-prosumer systems, respectively. As can be seen, the required available capacities, ΔE, of the batteries are reduced when T_f increases. In addition, the required ΔE of the secondary ESDs are plotted in Figures 7b and 8b. The required available capacity ΔE of the battery is reduced by the SC/flywheel, since the secondary ESD responds to the high-frequency power demand. If there is no energy exchange between the primary and secondary ESDs, the total ΔE of the HESS should preferably be the same as that of the single-battery ESS (assuming other losses to be equal). Nevertheless, due to the unavoidable time delay in the power flow, the total ΔE of the HESS is larger than that of the single-battery ESS, which implies that the HESS is oversized.

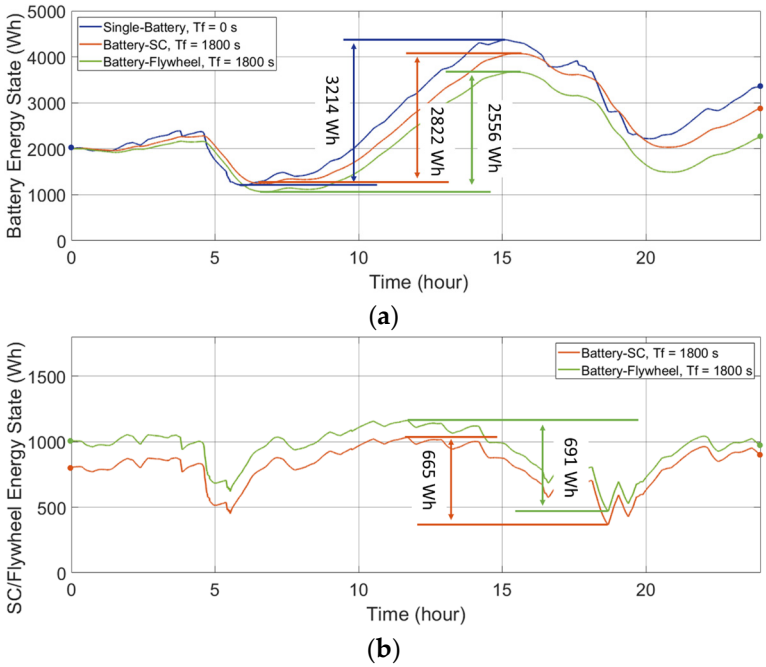


Figure 7. Energy states of the ESDs in the single-battery ESS and the HESSs applied to a wind-powered household-prosumer system. (**a**) Battery energy state. (**b**) SC/flywheel energy state.

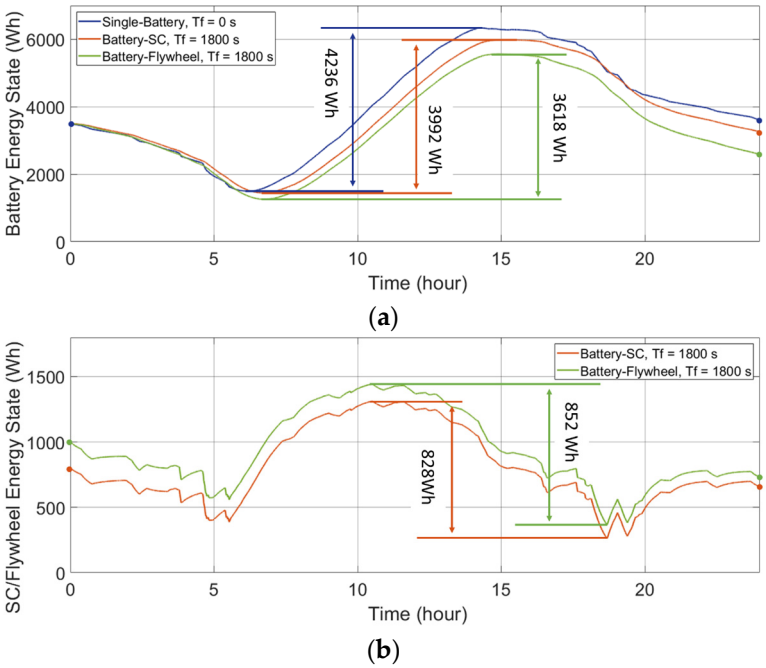


Figure 8. Energy states of the ESDs in the single-battery ESS and the HESSs applied to a PV-powered household-prosumer system. (**a**) Battery energy state. (**b**) SC/flywheel energy state.

Furthermore, the loss originates in the DC/DC converters and the ESDs. The amplitudes of the battery power and the SC/flywheel power ($|P_{bat}|$ and $|P_{SC/flywheel}|$) determine the losses of the converters and the cycle losses of the ESDs. The increased power flow caused by the unnecessary energy exchange leads to increased losses in the DC/DC converters. In addition, the cycle losses of the ESDs increase due to the increased throughput power of the ESDs. Additionally, the self-discharge loss of the SC/flywheel affects the loss of the HESS. The energy loss of the HESS is calculated from the components and is

reflected in the initial points and the end points of the energy curves (see Figures 7 and 8). The losses in different ESS combinations are listed in Table 1.

Table 1. Losses in different ESS combinations.

ESS/HESS (T_f = 1800 s)		Loss in Converters	Cycle Loss of ESDs	Self-Discharge Loss of ESDs	Total Loss in ESS/HESS
Wind-powered	Single-battery ESS	514 Wh	68 Wh	47Wh	629 Wh
	Battery-SC HESS	671 Wh	107 Wh	116 Wh	894 Wh
	Battery-flywheel HESS	717 Wh	142 Wh	727 Wh	1586 Wh
PV-powered	Single-battery ESS	538 Wh	72 Wh	49 Wh	659 Wh
	Battery-SC HESS	793 Wh	158 Wh	97 Wh	1048 Wh
	Battery-flywheel HESS	765 Wh	152 Wh	823 Wh	1740 Wh

Therefore, the unnecessary energy exchange between the primary and the secondary ESDs mainly results in two consequences:

1. The required capacity of the HESS is increased. Some of the capacity is wasted on the energy exchange within the HESS, and thus the HESS needs to be oversized.
2. There is a larger energy loss due to the increased power flows in the HESS.

In this paper, a low-pass filter controller was applied to explore the impact of the energy exchange between the ESDs on HESSs. Nevertheless, the phase shift is unavoidable in other liner filters.

Another important factor that affects HESSs is the time constant of the low-pass filter controller. It determines the power distribution of the HESS and the time delay of the power flow. Here, the battery-SC HESS in the wind-powered household-prosumer system is shown as an example to analyze the impact of the time constant. Figure 9 shows the power flows of the ESDs corresponding to different T_f in the low-pass filter. It can be seen that the time delay increases when T_f. increases. The larger time intervals $\Delta t'_1$ and $\Delta t'_2$ indicate that the power handled by the primary ESD is lower and smoother. Meanwhile, the secondary ESD handles more of the power peaks. The corresponding energy states of the ESDs are shown in Figure 10.

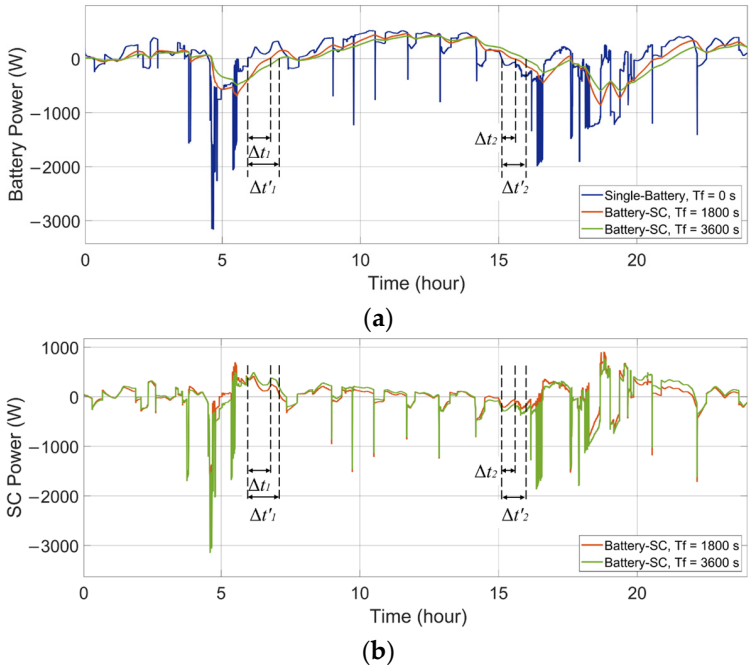


Figure 9. Power flows of the ESDs in the battery-SC HESS with different time constants in a wind-powered household-prosumer system. (**a**) Battery power. (**b**) SC power.

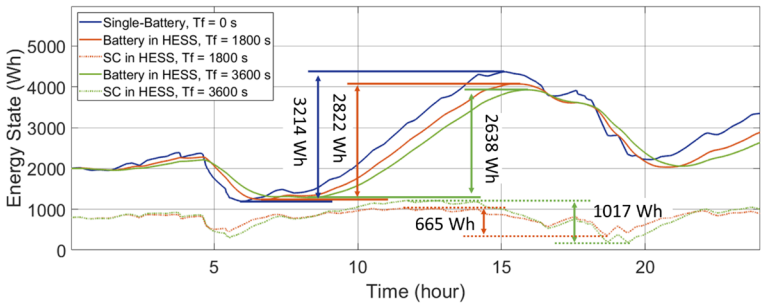


Figure 10. Energy states of the ESDs in the battery-SC HESS with different time constants in a wind-powered household-prosumer system.

Although the required ΔE of the battery decreases with a larger T_f, the total required ΔE of the HESS increases since the increased time delay increases the energy exchange between the ESDs. Here, in the single-battery ESS, a battery with 3214 Wh of available capacity meets the power demand. However, with T_f set to 1800 s and 3600 s in the battery-SC HESS, the required total ΔE increases to 3487 Wh and 3655 Wh, respectively. Thus, the required capacity of the HESS increases with the increasing T_f. In addition, due to the increased energy exchange within the HESS, the throughput powers of the ESDs increase. Thus, the energy loss of the HESS increases with increased T_f. The results are listed in Table 2.

Table 2. Comparison of the ΔE and the losses of the ESDs with different time constants.

ESS/HESS	Battery ΔE	SC ΔE	Total ΔE	Increase	Loss in Converters	ESD Cycle Loss	ESD Self-Discharge Loss	Total Loss
Single-battery	3214 Wh	-	3214 Wh	-	514 Wh	68 Wh	47 Wh	629 Wh
HESS (T_f = 1800 s)	2822 Wh	665 Wh	3487 Wh	9%	671 Wh	107 Wh	116 Wh	894 Wh
HESS (T_f = 3600 s)	2638 Wh	1017 Wh	3655 Wh	14%	783 Wh	139 Wh	125 Wh	1047 Wh

3.2. Experimental Setup

A battery-SC HESS experimental setup was utilized to verify the simulation results. The scaled-down prototype (see Figure 11) used a 20 volts DC bus. A power supply was used to emulate the RES power and a DC electronic load was implemented to emulate the load profiles of the user demand. The HESS consisted of a Li-ion battery pack and a SC pack with a total capacity of 216 Wh. The bi-directional DC/DC converter was made up of two MOSFETs, two capacitors, and an inductor. The nominal parameters of the experimental devices are given in Table 3.

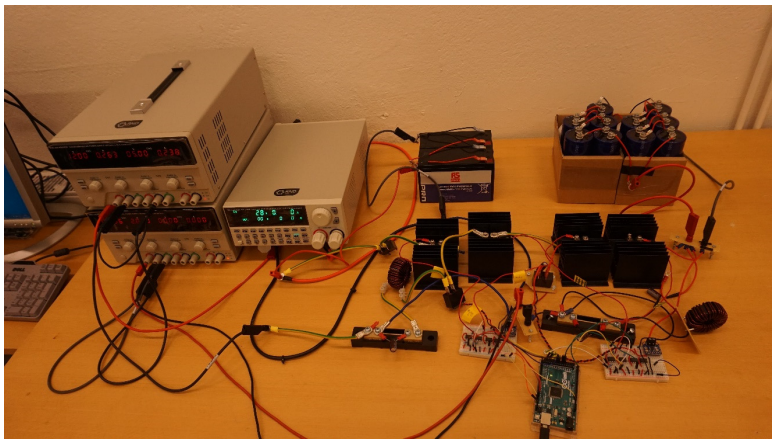


Figure 11. HESS experimental setup.

Table 3. Nominal parameters of the experimental devices.

Devices	Specifications
RES power emulator	Programmable power supply: RND 320-KD3305P [27]
Load power emulator	Programmable DC electronic load: RND 320-KEL102 [28]
Battery cell	12.8 V/7.5 Ah ×2 cells, 192 Wh, RS PRO Lithium Iron Phosphate Battery [29]
Supercapacitor cell	2400 F/2.7 V ×12 cells, 24 Wh, RND Radial Super Capacitor [30]
DC/DC converter	Switching frequency: 62.5 kHz, C = 1000 µF, L = 174 µH, MOSFET: IRL2505PBF-MOSFET N [31]

The measured currents of the batteries and the SCs in the single-battery ESS and the battery-SC HESSs are shown in Figures 12 and 13. The low-pass filter controller splits the demand current into low- and high-frequency parts. The SC responds to the high-frequency peaks in the demand and the battery is protected from large current fluctuations. There is a time delay between the battery current and the original demand current. In some time intervals, the battery charges and the SC discharges; this can be interpreted as the ESDs delivering energy to each other, which is unnecessary. In addition, when T_f increases from 1800 s to 3600 s, the battery current is smoother while the SC handles more power peaks. The time delay of the battery current is larger with the larger T_f.

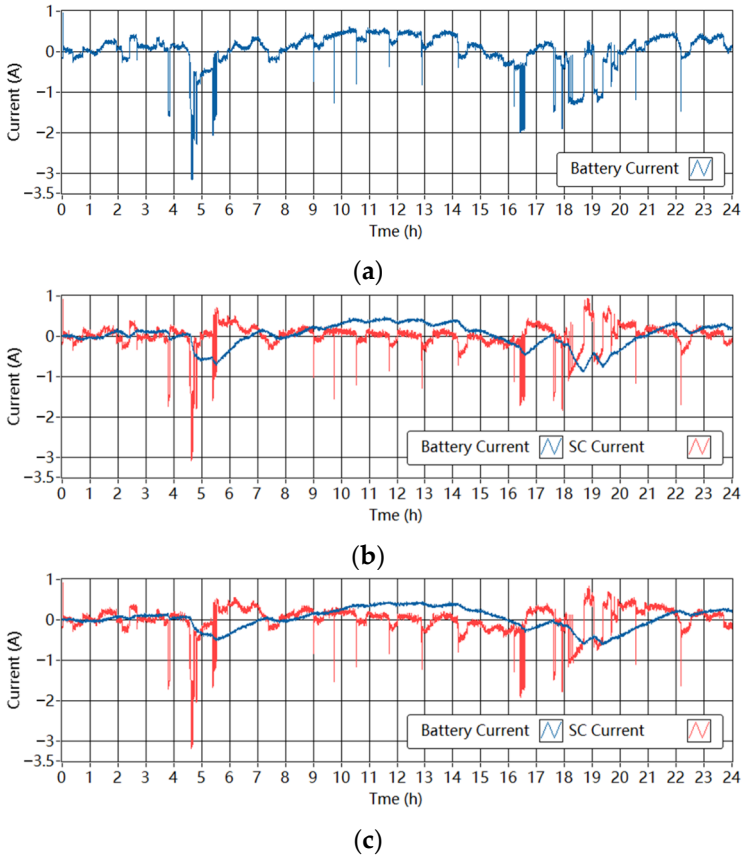


Figure 12. Measured currents through the ESDs in the experimental setup in the wind-powered system. (**a**) Single-battery ESS (**b**) Battery-SC HESS when T_f is 1800 s. (**c**) Battery-SC HESS when T_f is 3600 s.

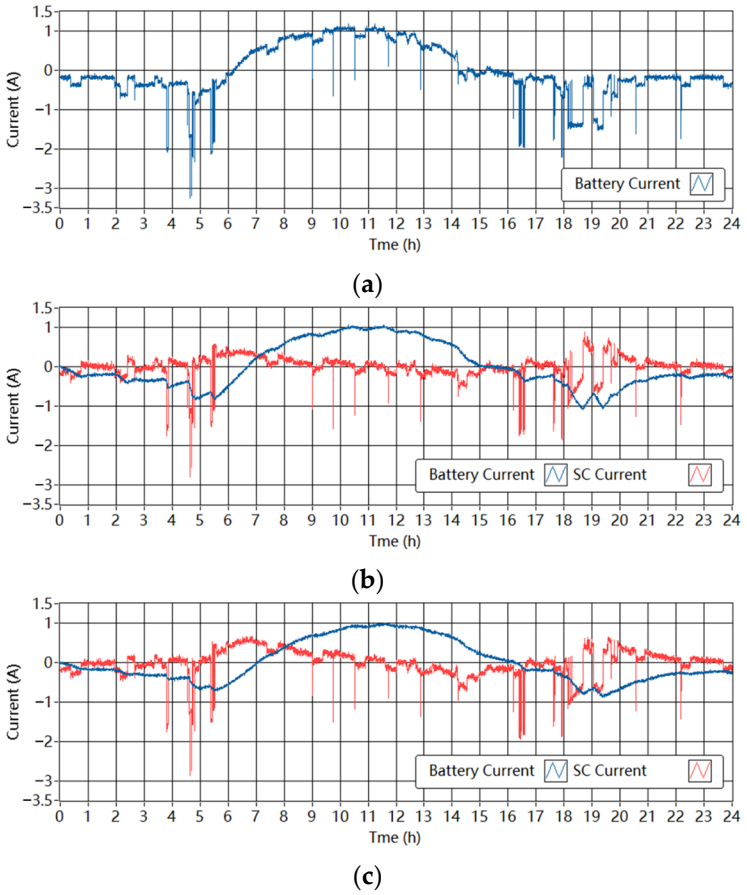


Figure 13. Measured currents through the ESDs in the experimental setup in the PV-powered system. (**a**) Single-battery ESS. (**b**) Battery-SC HESS when T_f is 1800 s. (**c**) Battery-SC HESS when T_f is 3600 s.

Figure 14 shows the corresponding SOC of the batteries and SCs in the single-battery ESS and the battery-SC HESSs in the wind-powered household-prosumer system. For the battery in the single-battery ESS, the minimum SOC was 0.41 and the maximum SOC was 0.73. The required ΔE of the battery in the setup is 61.4 Wh. In the HESSs, the SOC of the batteries changed less compared with the single-battery ESS. When T_f is 1800 s, the required ΔE of the battery and the SC in the HESS are 53.5 Wh and 12.7 Wh, respectively. Thus, the total required ΔE of the HESS (66.2 Wh) is about 8% larger than that of the single-battery ESS (61.4 Wh). In addition, when T_f increases to 3600 s, the required capacities of the battery and the SC are 51.1 Wh and 18.3 Wh, respectively. Thus, the total ΔE of the HESS increased from about 66 Wh to 69 Wh, which demonstrated an additional 5% increase and was approximately 12% larger than that of the single-battery ESS. In addition, Figure 15 shows the SOC of the batteries and SCs in the single-battery ESS and the battery-SC HESSs in the PV-powered household-prosumer system. The required ΔE of the battery in the single-battery ESS is 87.6 Wh. In the HESSs, the SOC of the batteries changed less compared with the single-battery ESS. When T_f is 1800 s, the required ΔE of the battery and the SC in the HESS are 78.3 Wh and 15.2 Wh, respectively. Thus, the total required ΔE of the HESS (93.5 Wh) is about 7% larger than that of the single-battery ESS (87.6 Wh). In addition, when T_f increases to 3600 s, the required capacities of the battery and the SC are 75.4 Wh and 20.8 Wh, respectively. Thus, the total ΔE of the HESS increased to about 96 Wh, which was 10% larger than that of the single-battery ESS. The measured results agreed with the simulation results.

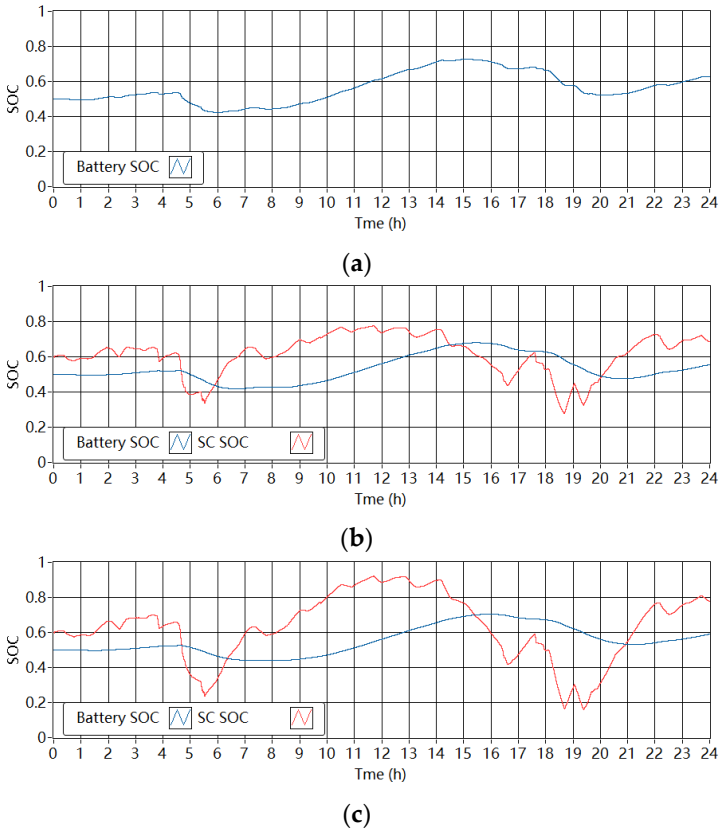


Figure 14. SOC of ESDs in the experimental setup in the wind-powered system. (**a**) Single-battery ESS. (**b**) Battery-SC HESS when T_f is 1800 s. (**c**) Battery-SC HESS when T_f is 3600 s.

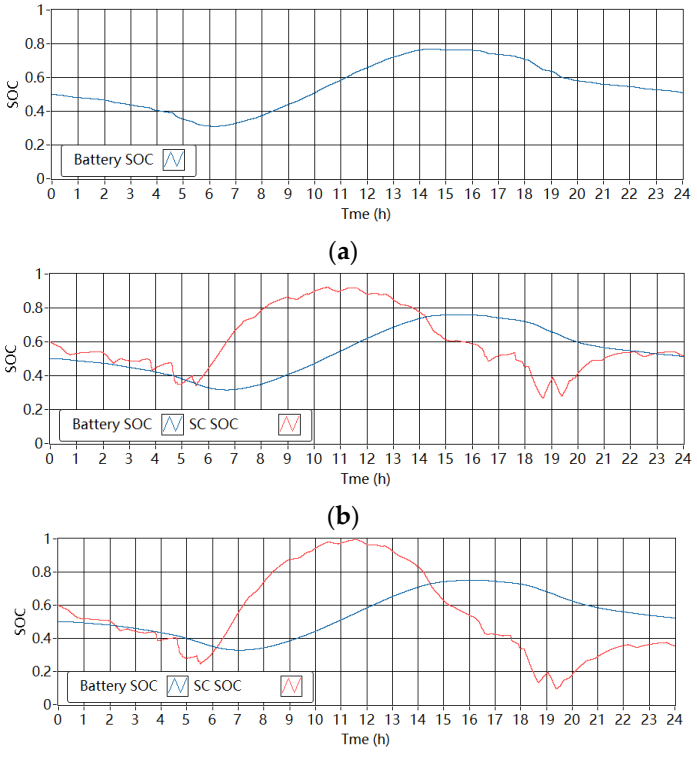


Figure 15. SOC of the ESDs in the experimental setup in the PV-powered system. (**a**) Single-battery ESS. (**b**) Battery-SC HESS when T_f is 1800 s. (**c**) Battery-SC HESS when T_f is 3600 s.

4. Comparison of Single-Battery ESS, Battery-SC HESS, and Battery-Flywheel HESS

The use of single-battery ESS, the battery-SC HESS, and the battery-flywheel HESS in RES prosumer systems are compared to discuss the impact of their respective energy exchange. For different individual households, the results are diverse due to different RESs and power consumption patterns. Thus, ten different power load profiles were chosen from the data set to give a range of different scenarios. The averages of the results are discussed in order to investigate the general trends.

In addition, there are several different chemistries in the Li-ion battery family, in which NMC batteries and LFP batteries account for a large share of the installed capacity of ESSs and electric vehicles. Although LFP batteries are inferior to NMC batteries in terms of energy density, LFP batteries offer advantages in terms of their lifetime and safety [32]. Therefore, the HESSs that respectively include the NMC battery and the LFP battery are investigated to estimate the battery lifetimes. Based on the required capacities of the ESDs and the lifetimes of the batteries, the project costs of different ESS combinations are then estimated.

4.1. Comparison Analysis

The variations of the maximum charging and discharging powers of the batteries in the HESSs with increasing T_f are plotted in Figure 16. T_f = 0 s indicates that the battery has to handle the entire power demand alone. Both the maximum charging and discharging powers of the batteries in the HESSs decline with increasing T_f because the secondary ESD handles more of the power demand and reduces the stress on the battery.

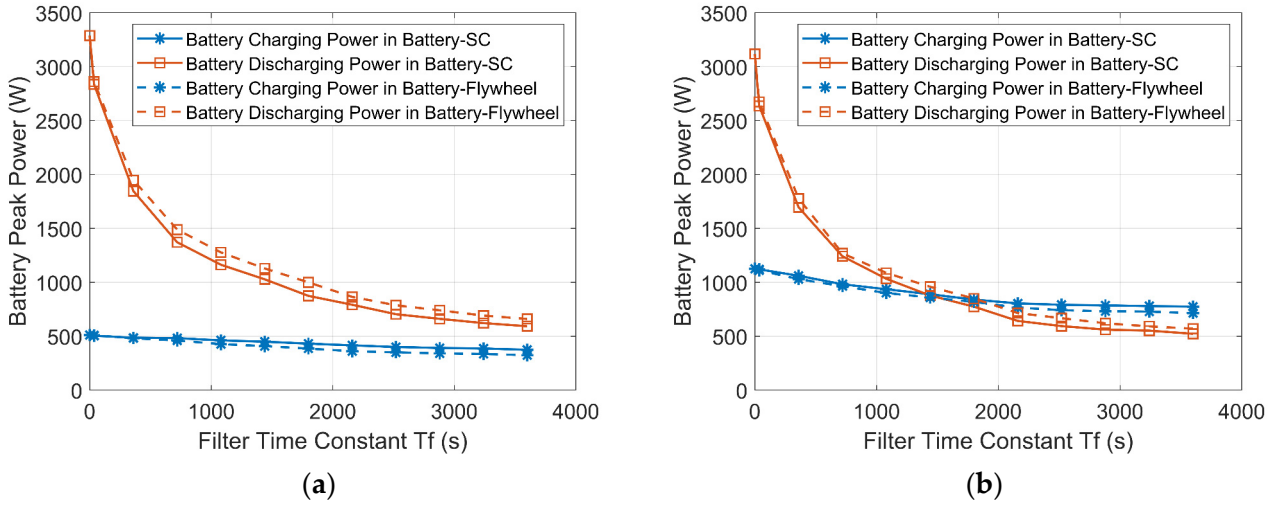


Figure 16. Variations of the maximum battery charging power and discharging power with increasing T_f. (**a**) Wind-powered household-prosumer system. (**b**) PV-powered household-prosumer system.

Figure 17 demonstrates how the energy losses of the HESSs increase with increasing T_f as a result of the increased energy exchange between the ESDs. In addition, the energy loss of the battery-flywheel HESS is higher than that of the battery-SC HESS due to the higher self-discharge rate of the flywheel.

The comparison of the ΔE and the capacities of the ESDs are plotted in Figures 18 and 19. As shown by the solid lines, with increasing T_f in the low-pass filter controller, the ΔE of the batteries (solid blue lines) decreases in both the battery-SC HESS and the battery-flywheel HESS. However, the energy exchange between the ESDs increases due to the increased time delay of the power flow. As a consequence, the ΔE of the SC/flywheel (solid red lines) and the sum of the ΔE of the ESDs (solid green lines) increase with increasing T_f.

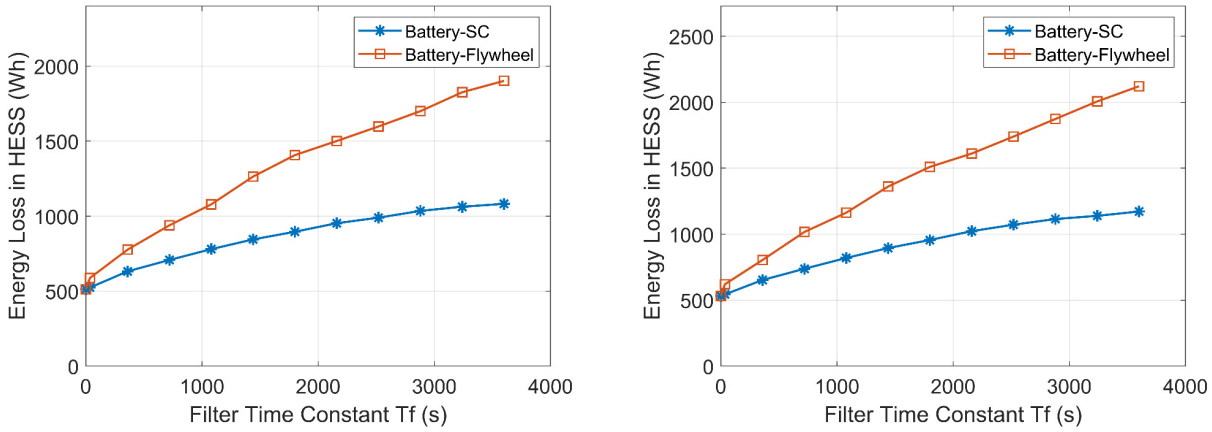


Figure 17. Variations of the energy losses of the HESSs with increasing T_f. (**a**) Wind-powered household-prosumer system. (**b**) PV-powered household-prosumer system.

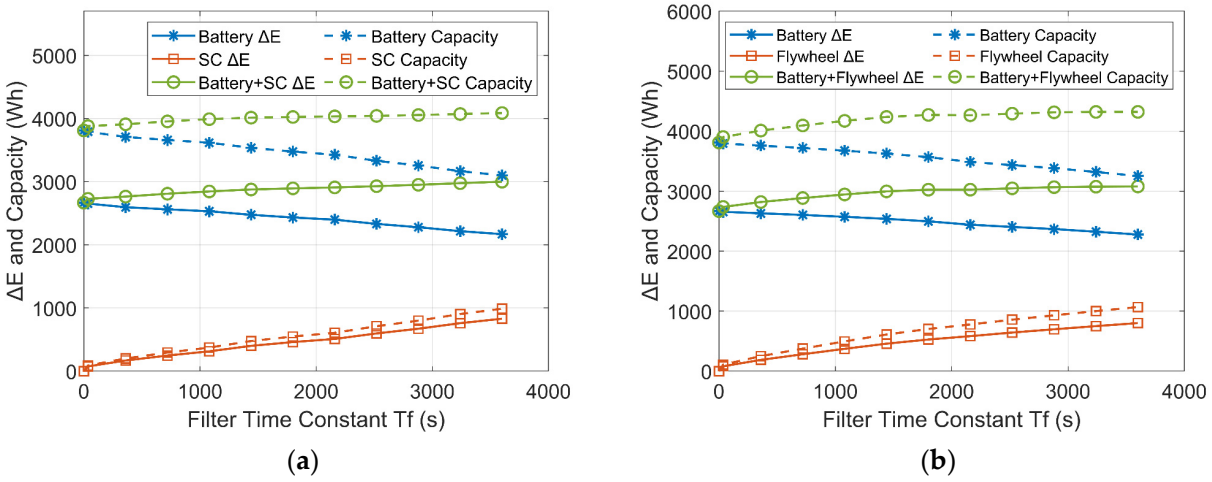


Figure 18. Variations of ΔE and capacities of the ESDs with increasing T_f in a wind-powered household-prosumer system. (**a**) Battery-SC HESS. (**b**) Battery-flywheel HESS.

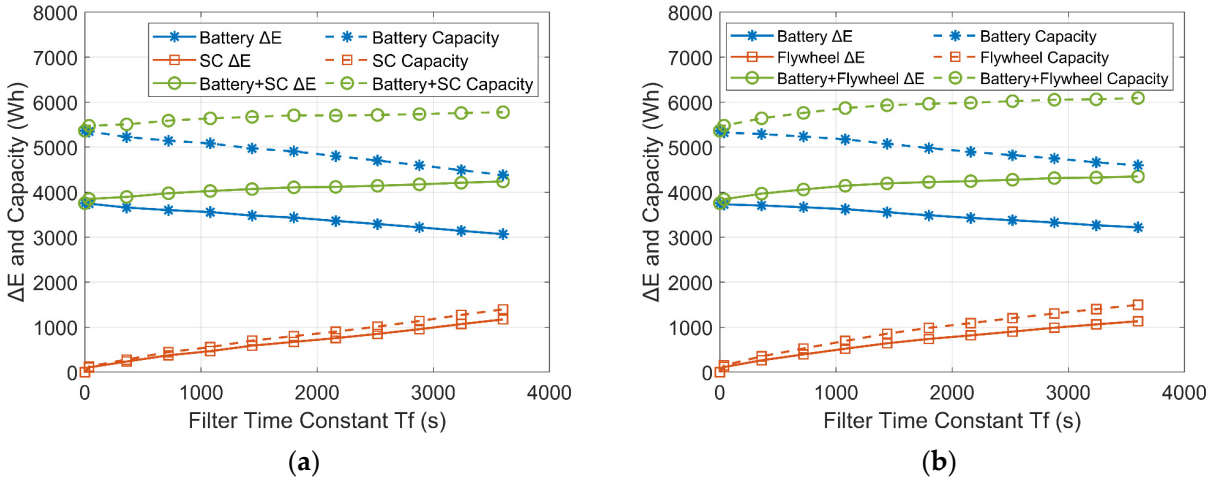


Figure 19. Variations of ΔE and capacities of the ESDs with increasing T_f in a PV-powered household-prosumer system. (**a**) Battery-SC HESS. (**b**) Battery-flywheel HESS.

In addition, the available SOC range limits the available capacities of the ESDs, where SOCmax and SOCmin are the upper and lower limits. To avoid a rapid capacity degradation during operations with a large depth of discharge (DOD), the available SOC range of the battery is set between 20% and 90% [33]. In addition, the available SOC of the SC is set between 16% and 100% (V_{SC_min} = $0.4V_{SC_max}$) [34]. The flywheel operates between 25% and 100% SOC (the lowest rotation speed is half of the highest rotation speed) [35]. Therefore, the actual required installed capacity of the ESD Q_{ESD} is written as:

$$Q_{ESD} = \frac{\Delta E}{SOC_{\max} - SOC_{\min}} \tag{8}$$

The dashed lines show that the actual capacities of the ESDs correspond to their ΔE and feature similar trends to ΔE. When T_f is 3600 s, both the total capacities of the battery-SC HESS and the battery-flywheel HESS are larger than that of the single-battery ESS. In addition, the installed capacity of the battery-SC HESS is slightly less than that of the battery-flywheel HESS due to the relatively low self-discharge rate of the SCs compared to the flywheels.

Furthermore, the installed capacity of the HESSs in the PV-powered household-prosumer system is larger than that in the wind-powered system. The PV-powered system only generates power during the day. This means that it needs a larger ESS to be able to shift energy compared with the wind-powered system.

Generally speaking, on one hand, the SC/flywheel distinctly reduces the charge/discharge current rate and the capacity of the battery, which predictably extends the battery's lifetime and reduces the cost of the battery pack. On the other hand, because some parts of the capacities of the ESDs are used to deliver energy between each other within the HESS, the reduction of the battery's capacity is less than the capacity of the secondary ESD that increases. Therefore, the total capacity of the HESS exceeds that of the single-battery ESS, which indicates a higher initial investment cost for the HESS. In addition, the increased energy loss of the HESS, which is caused by the increased power flow and the high self-discharge of the SC/flywheel, leads to decreased energy efficiency.

4.2. Battery Lifetime Estimation

The characteristics of capacity fading in batteries and estimations of battery lifetimes have been studied in many papers (e.g., [36,37]). When their capacity reaches 80% of the nominal capacity, batteries are usually determined to have the end-of-life stage and to require replacement.

For the NMC battery, an empirical model for capacity degradation is obtained by curve fitting from the reference [38]:

$$Q_{loss,\%} = \underbrace{14876 \cdot (t)^{0.5} \cdot \exp\left(\frac{-24.5kJ}{RT}\right)}_{\text{Calender aging model}} + \underbrace{(0.0008\exp(0.3903 \cdot C\text{-}rate)) \cdot Ah_{throughput}}_{\text{Cycle aging model}}. \tag{9}$$

The empirical aging model used in this study to estimate the lifetime of the LFP battery is from [39]:

$$Q_{loss} = \underbrace{3.087 \cdot 10^{-7} \cdot \exp(0.05146 \cdot T) \cdot (t/30)^{0.5}}_{\text{Calender aging model}} + \underbrace{6.87 \cdot 10^{-5} \cdot \exp(0.027 \cdot T) \cdot \left(\frac{Ah_{throughput}}{2 \cdot Capacity}\right)^{0.5}}_{\text{Cycle aging model}} \tag{10}$$

$$Ah_{throughput} = \int_0^{24 \cdot t} |I_{bat}| dt \tag{11}$$

where the *C-rate* is the current rate of the battery being charged or discharged, t represents the operating time of the battery (in days), R is the gas constant (8.314 J/(mol·K)), and T is the temperature in K. The ambient temperature for the estimation is considered as 25 °C (293.15 K). $Ah_{throughput}$ is chosen as the parameter for the aging model because it represents the amount of energy delivered by the battery. The $Ah_{throughput}$ is calculated by the current throughput from the battery for the whole operating time (in hours). The lifetimes of the NMC battery and the LFP battery that are estimated by these two models include both cycle aging and calendar aging.

Figure 20 shows the distribution of the battery current rates for one of the test cases in the wind-powered household-prosumer system. Compared with the single-battery ESS, the batteries in both the HESSs experience lower C-rates, which avoids the need for the high C-rates to charge and discharge. With the lower C-rates, the total Ah-throughput of the batteries is significantly lower than that of the single-battery ESS. Consequently, the HESSs reduce the equivalent full cycles (EFC) of the batteries, which slows down cycle aging. In addition, for the battery-flywheel HESS, since the self-discharge loss of the flywheel is larger than that of the SC, the battery discharges more often. Thus, the frequency of the discharge current is slightly higher than that of the battery-SC combination.

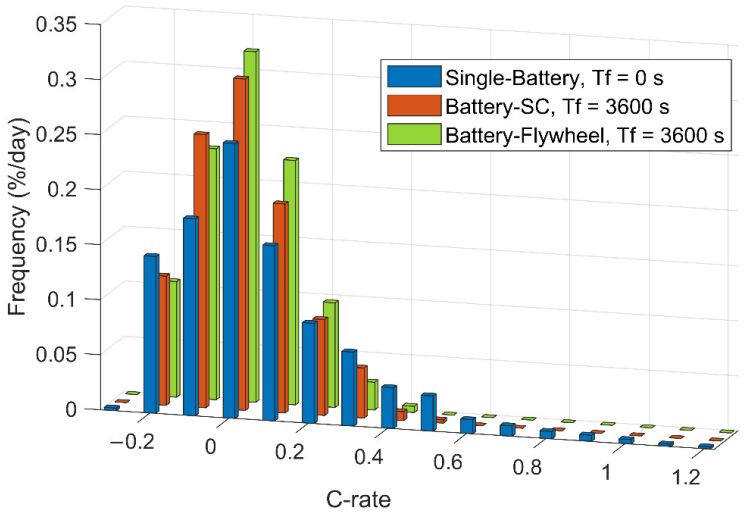


Figure 20. Distribution of the battery current rates during one day in a wind-powered household-prosumer system (0 C is the interval between ±0.04 C).

Utilizing the distribution of the C-rates and the total EFC, the battery lifetimes are estimated. As shown in Figure 21, the SC/flywheel reduces the stress on the battery and increases the battery lifetime. The extension of the battery lifetime in the battery-SC HESS is close to that of the battery-flywheel HESS. It can be seen that the lifetime of the LFP battery is much longer than that of the NMC battery. Compared with the single-LFP battery ESS, the lifetimes of the LFP batteries in the HESSs are extended by more than a quarter of the initial lifetime. In addition, although the capacity of the battery is larger in the PV-powered system compared with the wind-powered system, the lifetimes of the batteries in the two RES household-prosumer systems are comparable due to the similar total EFCs in these two systems.

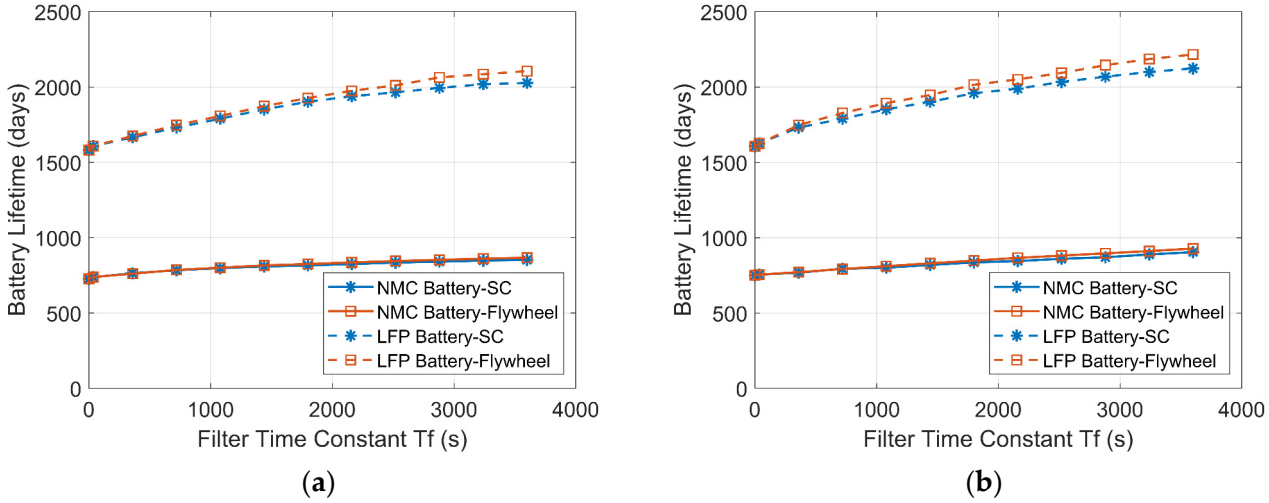


Figure 21. Estimate lifetimes of batteries in the HESSs with increasing time constant. (**a**) Wind-powered household-prosumer system. (**b**) PV-powered household-prosumer system.

4.3. Cost Analysis

Because the target of the analysis is to compare the HESSs, the cost analysis only concerns the costs of the ESDs along with the bi-directional DC/DC converters. The costs of the RESs and the other components in the system are not discussed. In addition, the cost analysis highly depends on the lifetimes and the capacity costs of the different energy storage technologies. Compared with the capital cost, the operating and maintenance costs of the ESDs are negligible and are, thus, neglected [40]. The simplified cost calculation includes the cost of the battery C_{bat}, the cost of the SC/flywheel $C_{SC/fly}$, and the cost of the converter C_{con}:

$$C_{total} = C_{bat} + C_{SC/fly} + C_{con} \tag{12}$$

$$\begin{cases} C_{bat} = \left\lceil \frac{t}{t_{bat}} \right\rceil \cdot (Q_{bat} c_{bat}) + c_{ins_bat} \\ C_{SC} = Q_{SC} c_{SC} + c_{ins_SC} \\ C_{fly} = Q_{fly} c_{fly} + c_{ins_fly} \\ C_{con} = n P_{con} c_{con} \end{cases} \tag{13}$$

where t is the project's operating time in years (up to 30 years) and t_{bat} is the lifetime of the battery in years. Using the ceiling value of the t/t_{bat} represents the investment times of the battery (i.e., including the initial cost and replacement cost), Q_{bat} is the capacity of the battery, c_{bat} is the Li-ion battery cost per kWh, and c_{ins_bat} is the installation cost of the battery. For the SC, Q_{SC} is the capacity of the SC, c_{SC} is the SC cost per kWh, and c_{ins_SC} is the installation cost. For the flywheel, Q_{fly} represents the capacity of the flywheel, c_{fly} represents the flywheel cost per kWh, and c_{ins_fly} represents the installation cost. For the bi-directional DC/DC converter, n is the number of the converters (n = 1 in the single-battery ESS and n = 2 in the HESS), P_{con} is the nominal power of the converter (5 kW is used here), and c_{con} is the cost (per kW) of the converter.

Taking into account the costs of NMC batteries and LFP batteries reported in published research [40–42], the parameters are summarized to analyze the project cost. In addition, the retail price in the C.A.R.M.E.N. market report is considered [43]. The parameters for the cost estimation are shown in Table 4.

Table 4. Nominal parameters of the experimental devices.

Parameters	Value	Unit	Source
$c_{_bat_NMC}$	495	€/kWh	[40–43]
$c_{_bat_LFP}$	420	€/kWh	[40–43]
c_{ins_bat}	200	€	Assumption
$c_{_SC}$	10,000	€/kWh	[44]
c_{ins_SC}	200	€	Assumption
$c_{_fly}$	2815	€/kWh	[40]
c_{ins_fly}	1000	€	Assumption
$c_{_con}$	150	€/kW	[45]

The exchange rate between the euro and US dollar is used as 0.86 when parameters are converted from the references.

The results of the estimated battery lifetimes and project costs of the HESSs are listed in Table 5. The results highlight that the initial cost of both the battery-SC HESS and the battery-flywheel HESS is clearly higher than that of the single-battery ESS due to the oversized capacity of the HESS, the high price of the SC/flywheel, and the cost of an additional DC/DC converter. With a 30 year project lifetime, the single-LFP battery ESS shows the lowest total cost as a result of the longer battery lifetime of the LFP battery compared with the NMC battery. For the battery-SC HESS with either the NMC battery or the LFP battery, although the lifetime of the battery is extended, the total project cost of the battery-SC combination is higher than that of the single-battery ESS with the same type of batteries. This is caused by the current high cost of SCs. Furthermore, the project cost of the battery-flywheel HESS is comparable to that of the single-battery ESS. The project cost of the NMC battery-flywheel HESS is less than that of the single-NMC battery ESS since the NMC battery needs to be replaced relatively often and the replacement cost of the battery part is relatively high. Conversely, when the HESS employs LFP batteries as the primary ESD, the project cost of the LFP battery-flywheel HESS is slightly larger than that of the single-LFP battery ESS. The variations in the costs of these HESSs over 30 years are shown in Figure 22.

Table 5. Battery lifetime estimation and cost of the energy storage system (30 years project lifetime).

ESS Combination		Battery Lifetime	Lifetime Extension	Initial Cost	Total Cost	Cost Increase
Wind-powered	Single-NMC battery	725 days/2.0 years	-	2836 €	31,072 €	-
	NMC battery-SC HESS	853 days/2.3 years	18%	13,317 €	31,746 €	674 €
	NMC battery-flywheel HESS	868 days/2.4 years	20%	7318 €	26,681 €	−4391 €
	Single-LFP battery	1581 days/4.3 years	-	2550 €	12,157 €	-
	LFP battery-SC HESS	2027 days/5.6 years	28%	13,084 €	19,582 €	7425 €
	LFP battery-flywheel HESS	2092 days/5.7 years	32%	7073 €	13,905 €	1748 €
PV-powered	Single-NMC battery	751 days/2.1 years	-	3605 €	40,763 €	-
	NMC battery-SC HESS	904 days/2.5 years	20%	18,019 €	44,037 €	3274 €
	NMC battery-flywheel HESS	928 days/2.5 years	24%	9257 €	35,028 €	−5735 €
	Single-LFP battery	1628 days/4.5 years	-	3205 €	16,419 €	-
	LFP battery-SC HESS	2124 days/5.8 years	30%	17,690 €	26,891 €	10,472 €
	LFP battery-flywheel HESS	2215 days/6.1 years	36%	8843 €	16,573 €	154 €

The stepwise increasing lines indicate that the project costs increase when the batteries need to be replaced. The general conclusions from the cost analysis are as follows:

1. The project costs show similar trends in both the wind-powered system and PV-powered system, where the NMC battery-SC HESS has the highest project cost and the single-LFP battery ESS has the lowest project cost.
2. The costs for HESSs that include LFP batteries are visibly lower than those of the corresponding HESSs with NMC batteries.
3. Although HESSs are initially more costly, their cost increases relatively slowly compared to the single-battery ESSs due to the extended lifetime of the battery in HESSs.

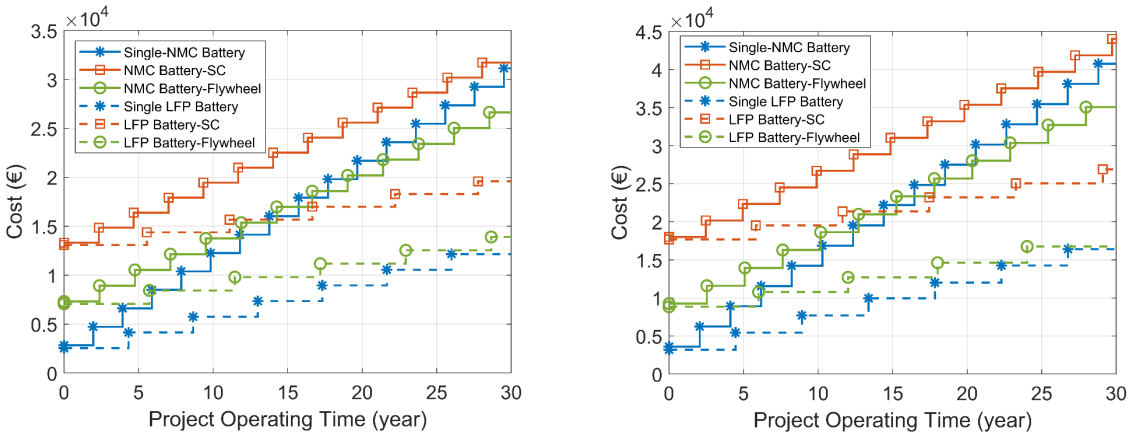


Figure 22. Costs of the single-battery ESS, the battery-SC HESS, and the battery-flywheel HESS over 30 years (T_f is 3600 s). (**a**) Wind-powered household-prosumer system. (**b**) PV-powered household-prosumer system.

With the development of the battery market caused by increasing RESs and electric vehicles, the cost of Li-ion batteries is continuously decreasing. Therefore, the selection of the appropriate ESS solution in the RES household-prosumer system should be performed carefully, using a techno-economic analysis for the different technologies involved and the planned project lifetime.

5. Conclusions

Through an analysis of the energy exchange caused by the phase shift of the low-pass filter controller, this study discussed the cause of the oversized capacity and increased energy loss of the HESS. The unnecessary energy exchange implies that some of the capacity is used to deliver energy within the HESS instead of serving the DC bus. Thus, the total capacity of the HESS that is required to meet the demand is distinctly larger than that of the single-battery ESS. Moreover, the energy loss of the HESS is larger than that of the single-battery ESS due to the larger throughput powers of the individual ESDs and the high self-discharge rate of the SC/flywheel. In addition, the increased time constant of the filter controller causes both the required capacity and the energy loss of the HESS to increase. Furthermore, although the battery lifetime is extended by the secondary ESD, the single-battery ESS demonstrates an initial cost advantage compared with the HESS, since its required capacity is lower. Due to the longer lifetime of LFP batteries, the single-LFP battery ESS features the lowest project cost. However, the cost over time of the battery-flywheel HESS is comparable to that of the single-battery ESS for a 30 year project lifetime. The cost advantage of the HESS will become clear over time if the project is designed for long-term usage. The techno-economic analysis for the different ESSs/HESSs depends on the specific project situation and lifetime.

Author Contributions: Conceptualization, Y.J. and D.M.; data curation, Y.J.; formal analysis, Y.J.; funding acquisition, D.M.; investigation, Y.J.; methodology, Y.J. and D.M.; project administration, D.M.; resources, D.M.; software, Y.J.; supervision, D.M.; validation, Y.J. and D.M.; visualization, Y.J.; writing—original draft, Y.J.; writing—review and editing, D.M. All authors have read and agreed to the published version of the manuscript.

Funding: This research was funded by the China Scholarship Council (CSC), and the StandUp for Energy Project via the Swedish Research Council.

Institutional Review Board Statement: Not applicable.

Informed Consent Statement: Not applicable.

Data Availability Statement: The data presented in this study are available on request from the corresponding author.

Conflicts of Interest: The authors declare no conflict of interest.

References

1. Shahsavari, A.; Akbari, M. Potential of solar energy in developing countries for reducing energy-related emissions. *Renew. Sustain. Energy Rev.* **2018**, *90*, 275–291. [CrossRef]
2. Sun, C.; Negro, E.; Vezzù, K.; Pagot, G.; Cavinato, G.; Nale, A.; Bang, Y.H.; Di Noto, V. Hybrid inorganic-organic proton-conducting membranes based on SPEEK doped with WO3 nanoparticles for application in vanadium redox flow batteries. *Electrochim. Acta* **2019**, *309*, 311–325. [CrossRef]
3. Molina, M.G. Energy storage and power electronics technologies: A strong combination to empower the transformation to the smart grid. *Proc. IEEE* **2017**, *105*, 2191–2219. [CrossRef]
4. Vazquez, S.; Lukic, S.M.; Galvan, E.; Franquelo, L.G.; Carrasco, J.M. Energy storage systems for transport and grid applications. *IEEE Trans. Ind. Electron.* **2010**, *57*, 3881–3895. [CrossRef]
5. Hou, J.; Yang, M.; Wang, D.; Zhang, J. Fundamentals and challenges of lithium ion batteries at temperatures between −40 and 60 °C. *Adv. Energy Mater.* **2020**, *18*, 1904152. [CrossRef]
6. Zhang, H.; Sun, C. Cost-effective iron-based aqueous redox flow batteries for large-scale energy storage application: A review. *J. Power Sources* **2021**, *493*, 229445. [CrossRef]
7. Pugach, M.; Vyshinsky, V.; Bischi, A. Energy efficiency analysis for a kilo-watt class vanadium redox flow battery system. *Appl. Energy* **2019**, *253*, 113533. [CrossRef]
8. Díaz-González, F.; Sumper, A.; Gomis-Bellmunt, O.; Villafáfila-Robles, R. A review of energy storage technologies for wind power applications. *Renew. Sustain. Energy Rev.* **2012**, *16*, 2154–2171. [CrossRef]
9. Haruni, A.M.O.; Negnevitsky, M.; Haque, M.E.; Gargoom, A. A novel operation and control strategy for a standalone hybrid renewable power system. *IEEE Trans. Sustain. Energy* **2013**, *2*, 402–413. [CrossRef]
10. Mohamad, F.; Teh, J.; Lai, C.M.; Chen, L.R. Development of energy storage systems for power network reliability: A review. *Energies* **2018**, *11*, 2278. [CrossRef]
11. Kotra, S.; Mishra, M.K. Design and stability analysis of dc microgrid with hybrid energy storage system. *IEEE Trans. Sustain. Energy* **2019**, *10*, 1603–1612. [CrossRef]
12. Lu, X.; Chen, Y.; Fu, M.; Wang, H. Multi-objective optimization-based real-time control strategy for battery/ultracapacitor hybrid energy management systems. *IEEE Access* **2019**, *7*, 11640–11650. [CrossRef]
13. Gee, A.M.; Robinson, F.V.P.; Dunn, R.W. Analysis of battery lifetime extension in a small-scale wind-energy system using supercapacitors. *IEEE Trans. Energy Convers.* **2013**, *28*, 24–33. [CrossRef]
14. Arani, A.A.K.; Gharehpetian, G.B.; Abedi, M. A novel control method based on droop for cooperation of flywheel and battery energy storage systems in islanded microgrids. *IEEE Syst. J.* **2020**, *14*, 1080–1087. [CrossRef]
15. Zimmermann, T.; Keil, P.; Hofmann, M.; Horsche, M.F.; Pichlmaier, S.; Jossen, A. Review of system topologies for hybrid electrical energy storage systems. *J. Energy Storage* **2016**, *8*, 78–90. [CrossRef]
16. Abbey, C.; Strunz, K.; Joos, G. A knowledge-based approach for control of two-level energy storage for wind energy systems. *IEEE Trans. Energy Convers.* **2009**, *24*, 539–547. [CrossRef]
17. Nguyen, C.L.; Lee, H.H. Optimization of wind power dispatch to minimize energy storage system capacity. *J. Elect. Eng. Technol.* **2014**, *9*, 1080–1088. [CrossRef]
18. Jing, W.; Lai, C.H.; Wong, S.; Wong, M. Battery-supercapacitor hybrid energy storage system in standalone DC microgrids: A review. *IET Renew. Power Gener.* **2017**, *11*, 461–469. [CrossRef]
19. Li, W.; Joos, G.; Belanger, J. Real-time simulation of a wind turbine generator coupled with a battery supercapacitor energy storage system. *IEEE Trans. Ind. Electron.* **2010**, *57*, 1137–1145. [CrossRef]
20. Chong, L.W.; Wong, Y.W.; Rajkumar, R.K.; Isa, D. Hybrid energy storage systems and control strategies for stand-alone renewable energy power systems. *Renew. Sustain. Energy Rev.* **2016**, *66*, 174–189. [CrossRef]
21. *MATLAB*; Version 9.7.0 (R2019b); The MathWorks Inc.: Natick, MA, USA, 2019.
22. Real Time Data, Sotavento. Available online: http://www.sotaventogalicia.com/en/real-time-data/historical (accessed on 5 September 2021).
23. PV Ladder Statistics. 2020. Available online: https://pvoutput.org/list.jsp?id=14676&sid=19720 (accessed on 5 September 2021).
24. Kolter, J.Z.; Johnson, M.J. Redd: A public data set for energy disaggregation research. In Proceedings of the SustKDD Workshop on Data Mining Applications in Sustainability, San Diego, CA, USA, 21–24 August 2011.
25. Huber, J.E.; Kolar, J. Applicability of solid-state transformers in today's and future distribution grids. *IEEE Trans. Smart Grid* **2019**, *10*, 317–326. [CrossRef]
26. Blanes, J.M.; Gutierrez, R.; Garrigos, A.; Lizan, J.L.; Cuadrado, J.M. Electric vehicle battery life extension using ultracapacitors and an FPGA controlled interleaved buck-boost converter. *IEEE Trans. Power Electron.* **2013**, *28*, 5940–5948. [CrossRef]
27. RND Programmable DC Power Supply, Datasheet RND 320-KD3305P. Available online: https://www.elfa.se/Web/Down-loads/_t/ds/RND%-20320-KD3305P_eng_tds.pdf (accessed on 5 September 2021).

28. RND Programmable DC Electronic Load, Datasheet RND 320-KEL102. Available online: https://www.elfa.se/Web/Downloads/_t/ds/RND%-20320-KEL102_eng_tds.pdf (accessed on 5 September 2021).
29. RS PRO Lithium Iron Phosphate Battery, Datasheet. Available online: https://docs.rs-online.com/c8bb/0900766b8172be40.pdf (accessed on 5 September 2021).
30. RND Radial Super Capacitor, Datasheet RND 150HP-2R7-J248UNJ50. Available online: https://www.elfa.se/Web/Down-loads/_t/ds/RND%-20150HP-2R7-J248UNJ50_eng_tds.pdf (accessed on 5 September 2021).
31. IRL2505PBF—MOSFET N, ELFA. Available online: https://www.elfa.se/en/mosfet-60-104-200-to-220-ir-irl2505pbf/p/17137722?q=MOSFET+N&pos=32&origPos=31&origPageSize=50&track=true (accessed on 5 September 2021).
32. Mulleriyawage, U.G.; Shen, W.; Hu, C. Battery system selection in dc microgrids for residential applications: An Australian case study. In Proceedings of the 14th IEEE Conference on Industrial Electronics and Applications (ICIEA), Xi'an, China, 19–21 June 2019.
33. Xu, B.; Oudalov, A.; Ulbig, A.; Andersson, G.; Kirschen, D. Modeling of lithium-ion battery degradation for cell life assessment. *IEEE Trans. Smart Grid* **2018**, *9*, 1131–1140. [CrossRef]
34. Petreus, D.; Moga, D.; Galatus, R.; Munteanu, R. Modeling and sizing of supercapacitors. *Adv. Electr. Comput. Eng.* **2018**, *8*, 15–22. [CrossRef]
35. Amiryar, M.E.; Pullen, K.; Nankoo, D. Development of a high-fidelity model for an electrically driven energy storage flywheel suit-able for small scale residential applications. *Appl. Sci.* **2018**, *8*, 453. [CrossRef]
36. Ecker, M.; Nieto, N.; Käbitz, S.; Schmalstieg, J.; Blanke, H.; Warnecke, A.; Sauer, D. Calendar and cycle life study of Li(NiMnCo)O2-based 18650 lithium-ion batteries. *J. Power Sources* **2014**, *248*, 839–851. [CrossRef]
37. Stroe, D.I.; Knap, V.; Swierczynski, M.; Stroe, A.I.; Teodorescu, R. Operation of a grid-connected lithium-ion battery energy storage system for primary frequency regulation: A battery lifetime perspective. *IEEE Trans. Ind. Appl.* **2017**, *53*, 430–438. [CrossRef]
38. Wang, J.; Purewal, J.; Liu, P.; Hicks-Garner, J.; Soukazian, S.; Sherman, E. Degradation of lithium ion batteries employing graphite negatives and nickel–cobalt–manganese oxide + spinel manganese oxide positives: Part 1, aging mechanisms and life estimation. *J. Power Sources* **2014**, *269*, 937–948. [CrossRef]
39. Stroe, D.I.; Swierczynski, M.; Stan, A.I.; Teodorescu, R.; Andreasen, S.J. Accelerated lifetime testing methodology for lifetime estimation of lithium-ion batteries used in augmented wind power plants. *IEEE Trans. Ind. Appl.* **2014**, *50*, 4006–4017. [CrossRef]
40. Zakeri, B.; Syri, S. Electrical energy storage systems: A comparative life cycle cost analysis. *Renew. Sustain. Energy Rev.* **2014**, *42*, 569–596. [CrossRef]
41. Chemali, E.; Preindl, M.; Malysz, P.; Emadi, A. Electrochemical and electrostatic energy storage and management systems for electric drive vehicles: State-of-the-art review and future trends. *IEEE J. Emerg. Sel. Top. Power Electron.* **2016**, *4*, 1117–1134. [CrossRef]
42. Ralon, P.; Taylor, M.; Ilas, A.; Diaz-Bone, H.; Kairies, K. *Electricity Storage and Renewables: Costs and Markets to 2030*; International Renewable Energy Agency: Abu Dhabi, United Arab Emirates, 2017.
43. CARMEN, Marktübersicht Batteriespeicher. 2020. Available online: https://www.carmen-ev.de/service/marktueberblick/marktueber-sicht-batteriespeicher (accessed on 5 September 2021).
44. Robyns, B.; Francois, B.; Delille, G.; Saudemont, C. *Energy Storage in Electric Power Grids*; ISTE-Wiley: London, UK, 2015; pp. 17–52.
45. Herrera, V.I.; Gaztanaga, H.; Milo, A.; de Ibarra, A.S.; Etxeberria-Otadui, I.; Nieva, T. Optimal energy management and sizing of a battery-supercapacitor-based light rail vehicle with a multiobjective approach. *IEEE Trans. Ind. Appl.* **2016**, *52*, 3367–3377. [CrossRef]